Wave numbers and Ar pressure-induced shifts of ^{198}Hg atomic lines measured by Fourier transform spectroscopy

2005 J. Phys. B: At. Mol. Opt. Phys. 38 3739

(http://iopscience.iop.org/0953-4075/38/20/009)

INSTITUTE OF PHYSICS PUBLISHING JOURNAL OF PHYSICS B: ATOMIC, MOLECULAR AND OPTICAL PHYSICS

J. Phys. B: At. Mol. Opt. Phys. **38** (2005) 3739–3753 doi:10.1088/0953-4075/38/20/009

Wave numbers and Ar pressure-induced shifts of ^{198}Hg atomic lines measured by Fourier transform spectroscopy

Damir Veza[1], **Marc L Salit, Craig J Sansonetti and John C Travis**

National Institute of Standards and Technology, Gaithersburg, MD 20899, USA

E-mail: veza@phy.hr

Received 8 July 2005, in final form 11 July 2005
Published 26 September 2005
Online at stacks.iop.org/JPhysB/38/3739

Abstract

Wave numbers and argon-pressure-induced shifts of mercury emission lines were measured using a UV/visible Fourier transform spectrometer (FTS). The observations were made with electrodeless lamps containing isotopically pure ^{198}Hg and argon buffer gas at pressures of 33 Pa (1/4 Torr), 400 Pa (3 Torr), 933 Pa (7 Torr) and 1333 Pa (10 Torr). Calibration of the FTS wave number scale was obtained from the four most prominent ^{198}Hg lines (6p $^3P_2$–7s $^3S_1$ at 546.2 nm, 6p $^3P_1$–7s $^3S_1$ at 436 nm, 6p $^3P_0$–7s $^3S_1$ at 404.8 nm and 6p $^3P_2$–6d $^3D_3$ at 365.1 nm), enabling measurements of wave numbers and argon pressure shifts of other UV and visible mercury transitions with high accuracy. Our measurements provide new data for the wave numbers and pressure-induced shifts of 20 mercury lines. The wave numbers of mercury lines emitted from the 400 Pa (3 Torr) lamp can be used as standards for wavelength calibration in inductively coupled plasma (ICP) spectrochemical analysis or in experiments where medium-resolution monochromators are used. The pressure-induced shifts of the ^{198}Hg emission lines are in reasonable agreement with theoretical predictions and could be of interest for validating calculations of mercury–argon interactions.

1. Introduction

Investigation of the spectrum of mercury has a long history. Various types of mercury discharge lamps are easy to make and operate, and mercury possesses a simple line spectrum. These characteristics made mercury low-pressure discharge lamps an attractive source for wavelength calibration in spectroscopy laboratories, especially after artificially made isotopically pure ^{198}Hg became available [1].

[1] Permanent address: Department of Physics, University of Zagreb, Zagreb, Croatia.

In the period 1950 to 1960, the strongest ^{198}Hg emission lines served as provisional primary wavelength standards [2]. Since that time there have been numerous research papers dealing with the accurate determination of the wavelengths of ^{198}Hg emission lines in the visible and UV part of the spectrum (see [3, 4] and references therein). Using Fabry–Perot interferometry Meggers and Kessler [3] made measurements of the wavelengths of 27 Hg emission lines relative to the mercury green line (transition 6p $^3P_2$–7s $^3S_1$ at 546 nm) using a water-cooled electrodeless lamp filled with isotopically pure ^{198}Hg and 3 Torr of argon buffer gas. Kaufman [4] used the same experimental technique to determine not only the wavelengths, but also the argon pressure-induced shifts of the 29 strongest mercury lines. Recently, interest in accurate measurements of the wavelengths and argon pressure shifts of ^{198}Hg emission lines has been revived because of the possibility of using its strongest lines as external wavelength standards for spectra of inductively coupled plasmas [5]. Furthermore, recent experiments show that the lines from low-pressure mercury lamps can be successfully used for the absolute and/or relative radiometric calibrations of spectrometers and detectors [6].

Today, four emission lines of ^{198}Hg (6p $^1P_1$–6d $^1D_2$ at 579 nm, 6p $^1P_1$–6d $^3D_2$ at 577 nm, 6p $^3P_2$–7s $^3S_1$ at 546 nm, and 6p $^3P_1$–7s $^3S_1$ at 436 nm) are recommended and widely used as secondary wavelength standards with a relative expanded uncertainty of about 5×10^{-8} [7]. The practical realization of these wavelength standards is an electrodeless lamp containing ^{198}Hg and argon at a low pressure (66 Pa to 133 Pa) to assure stable operation of the discharge [4, 7, 8]. Because these lamps are a practical laboratory tool by which wavelengths of unknown lines are determined in atomic and molecular spectra, an accurate knowledge of the transition wavelengths and a better knowledge of the argon pressure-induced shift of mercury atomic lines are of great practical interest.

It is interesting to note that mercury is a key constituent in chemically peculiar stars of the HgMn type [9]. Several mercury lines in the blue part of the spectrum (the Hg II transition $5d^96s^2\,^2D_{5/2}$–$5d^{10}6p\,^2P_{3/2}$ at 398.5 nm; two Hg I transitions 6p $^3P_0$–7s $^3S_1$ at 404.8 nm and 6p $^3P_1$–7s $^3S_1$ at 436 nm) are used by astronomers in the analysis of elemental and isotopic abundances relative to the solar chemical composition. An accurate knowledge of the wavelengths and the line profiles of these transitions is important for a reliable analysis of the diffusion processes in the stellar atmospheres.

Collision-induced shifts of atomic spectral lines are important properties that shed light on underlying atomic interactions. They are significant for fundamental as well as applied research in atomic physics and spectroscopy. Collision-induced shifts and widths have been investigated for decades, and several older reviews [10, 11, 12] cover early work in this field. There are also more recent, comprehensive surveys made by Lewis [13], Peach [14], and Allard and Kielkopf [15]. In addition, a rather complete bibliography covering experimental and theoretical research on pressure broadening and shift between 1978 and 1992 is available in an online database maintained by the National Institute of Standards and Technology (NIST) [16].

Collisional shifts and widths of spectral lines of metal atoms have been extensively studied, with particularly comprehensive work on broadening and shift of alkali lines by noble gases. Considerably less work has been reported on noble gas shift and broadening of atomic lines of more complex atoms such as mercury, despite their importance in basic and applied research. Data on the shift or broadening of the mercury resonance lines are more abundant than the data on all other mercury atomic lines, which are scarce or non-existent [13, 15]. We know of only one comprehensive set of measurements of the shifts of mercury atomic lines in the visible and near UV part of the spectrum [4]. Therefore, new or more accurate data on the shift of non-resonant mercury atomic lines are also of great interest.

The purpose of this paper is to present measurements of the wave numbers and pressure shifts of 20 lines of ^{198}Hg. In section 2 we describe our experimental set-up and the method of measurement. Section 3 is devoted to presenting and discussing our results for the measurements of wave numbers and pressure shifts of ^{198}Hg lines, as well as our calculations of pressure shifts of ^{198}Hg lines. We also compare our data with the results of other experiments. In section 4 we give conclusions based on the presented measurements and calculations.

2. Experiment

The experimental set-up comprises a Fourier transform spectrometer [17] and one of several low-pressure mercury electrodeless discharge lamps (EDL). The spectrometer is capable of operation in the spectral range 250 nm to 900 nm, but it is optimized for the violet/ultraviolet region. It is described in several recent papers covering its design [18, 19], operation [19, 5], and performance in the UV and visible spectral regions [20].

Sealed electrodeless discharge lamps, made of fused quartz and filled with a few milligrams of isotopically pure ^{198}Hg and pure argon, were used as the light sources. Two lamps were sealed (at room temperature) at each of four fixed pressures of argon: 33 Pa (1/4 Torr), 400 Pa (3 Torr), 933 Pa (7 Torr) and 1333 Pa (10 Torr). The lamps have a water-cooling jacket surrounding a narrow glass tube that contains the low-pressure mercury–argon plasma [20]. In the process of filling the lamps, the argon pressure was controlled by a capacitive manometer. The estimated uncertainty in the argon pressure does not exceed 1 Pa (10 mTorr) [20]. The lamps were excited by a microwave power supply delivering up to 120 W at a frequency of 2450 MHz. Coupling of the microwave power to the EDL was achieved by exciting the lamp in an Evenson-type cavity [21]. The lamp was mounted in front of the entrance aperture of the FTS, uniformly illuminating the aperture. The spectrum of each mercury EDL was observed in the UV (250 nm to 450 nm) and visible (380 nm to 650 nm) spectral ranges, with a typical resolution of 0.03 cm^{-1}.

In order to determine pressure shift rates and wave numbers under source conditions similar to those described in [4, 7], all measurements were performed at a fixed cooling water temperature of $(8 \pm 0.5)\,^{\circ}$C. At this temperature, the mercury vapour pressure was about 50 mPa (≈ 0.4 mTorr) [22] and the argon working pressure was about 4% lower than the nominal filling pressure at room temperature. This has been taken into account in the data analysis.

The FTS wave number scale was calibrated by using a multiplicative correction derived from four strong lines of ^{198}Hg I (transitions 6p ^{3}P$_2$–7s ^{3}S$_1$ at 546.2 nm, 6p ^{3}P$_1$–7s ^{3}S$_1$ at 436 nm, 6p ^{3}P$_0$–7s ^{3}S$_1$ at 404.8 nm, and 6p ^{3}P$_2$–6d ^{3}D$_3$ at 365.1 nm) as described in [20]. The wave numbers of these four internal standard lines were determined with high accuracy (relative standard uncertainty of about 1.2×10^{-8}) with respect to Doppler-free lines of molecular iodine [23] in a separate experiment [20].

We did not attempt to evaluate pressure broadening rates from these data because the FTS instrument function and Doppler broadening dominate the line shape and total line width, strongly masking the collisional contribution to the line width. Under these circumstances, deconvolution procedures cannot provide reliable data on the collisional line widths. However, accurate shift rates can be determined because the shift of a line is not affected by the FTS instrument function or the Doppler effect, which are symmetric broadening mechanisms.

3. Results and discussion

3.1. Wave numbers

In table 1 we present results of our measurements of wave numbers of ^{198}Hg atomic lines. In the first column, each line is identified by its approximate wavelength in nanometres.

Columns 2 and 3 specify the lower and upper levels involved in the transition. Measured wave numbers for lamps filled with argon at 400 Pa and 33 Pa are given in columns 4 and 6. In column 5 we also provide wavelengths for the 400 Pa lamp, since this lamp is most frequently used as a wavelength standard. For some lines the observed signal-to-noise (SNR) ratio was sufficient for accurate measurements in the 33 Pa lamp only. Finally, in the sixth column we give the wave numbers for the 20 strongest mercury lines extrapolated to zero argon pressure.

Figure 1 shows the pressure dependence for each line obtained by making a weighted linear least-squares fit to the data[2]. In addition to the intercept (the zero-pressure wave number), the regression analysis provides the pressure shift rate (PSR) for each line, the relative error of the pressure shift rate, and the upper and the lower confidence band limits for wave numbers calculated from the fitted zero-pressure wave number and PSR (dashed curves in figure 1). Most of the lines presented in the figure show a clear linear dependence of the shift on argon pressure, with a small scatter of data points. These lines have a high SNR in the observed spectra. Lines that show a large scatter of data points (for example the lines at 289.4 nm, 434.0 nm and 491.7 nm) also show the lowest SNR.

The experimental uncertainty of each wave number in table 1 is calculated as the quadrature sum of (a) the uncertainty in determining the position of the line centre, (b) the uncertainty in determining the multiplicative correction of the wave number scale and (c) a non-statistical relative uncertainty of 6.16×10^{-9}, which represents the limiting accuracy of the multiplicative correction for our FTS as determined in [20]. The uncertainties of strong lines (high SNR) are dominated by this last contribution, whereas the uncertainties of weak lines (low SNR) are dominated mostly by statistical variation. The uncertainties are combined to find the aggregate uncertainty in the wave number as $\Delta\sigma = \{(\Delta\sigma_a)^2 + (\Delta\sigma_b)^2 + (\Delta\sigma_c)^2\}^{1/2}$, representing one standard deviation. The uncertainties in table 1 have been expanded by a factor of 2 to provide a 95% confidence level.

The most comprehensive observations for spectral lines of ^{198}Hg were reported by Kaufman [4] who used Fabry–Perot interferometry to measure wavelengths of 29 lines in electrodeless discharge lamps filled with a small amount of ^{198}Hg and argon at room temperature pressures of 33 Pa, 400 Pa and 1333 Pa. The lamps were water cooled to temperatures of 6–9 °C. In figure 2, we compare wave numbers of ^{198}Hg lines measured in lamps with 33 Pa, 400 Pa and 1333 Pa argon in our experiment to the wave numbers measured at the same pressures by Kaufman [4]. The dashed lines represent the 95% confidence band limits for Kaufman's results based on his estimate of ±0.000 01 nm as the overall accuracy of his wavelength measurements. The error bars for each data point represent a 95% level of confidence for the wave numbers measured in our experiment. In general, the agreement between the two sets of measurements is satisfactory at the level of Kaufman's uncertainty. It appears, however, that our present results are systematically lower than those of Kaufman by about 0.0005 cm^{-1}.

The four ^{198}Hg lines marked with an 's' in table 1 are recommended as secondary wavelength standards by the International Committee for Weights and Measures (CIPM) [7]. These lines are of particular interest for the wavelength metrology community. The CIPM recommendations [7] specify working conditions for the practical realization of the definition of the metre. For our experiment all CIPM requirements (the lamp construction, the ^{198}Hg purity, the argon pressure in the lamp and the lamp working temperature) are

[2] The regression analysis has been performed using the 'R' statistical package. R is an integrated suite of software facilities for data manipulation, calculation and graphical display (see http://cran.r-project.org/doc/manuals/R-intro.pdf). Identification of this commercial software is made to adequately specify our procedures. Such identification does not imply recommendation or endorsement by the National Institute of Standards and Technology, nor does it imply that the products identified are necessarily the best available for the purpose.

Table 1. Wave numbers of ^{198}Hg emission lines measured at argon pressures of 400 Pa and 33 Pa, and the wave numbers corresponding to zero argon pressure (0 Pa column). Uncertainties are given at a 95% level of confidence.

Line name	Level		400 Pa		33 Pa	0 Pa	Notes[b]
	Lower	Upper	Wave number (cm^{-1})	Air wavelength[a] (nm)	Wave number (cm^{-1})	Wave number (cm^{-1})	
253.5	6p $^3P_0$	7d $^3D_1$			39 439.4819 (18)		
265.3	6p $^3P_1$	7d $^3D_2$			37 695.5599 (7)		
265.4	6p $^3P_1$	7d $^3D_1$			37 672.2624 (12)		
265.6	6p $^3P_1$	7d $^1D_2$			37 651.7291 (10)		
275.4	6p $^3P_0$	8s $^3S_1$			36 316.1334 (17)		
280.4	6p $^3P_2$	8d $^3D_3$			35 659.5707 (7)		
289.4	6p $^3P_1$	8s $^3S_1$	34 548.9191 (7)	289.359 831 (6)	34 548.9198 (6)	34 548.9199 (10)	
292.6	6p $^3P_2$	9s $^3S_1$			34 173.2024 (10)		
296.8	6p $^3P_0$	6d $^3D_1$	33 691.0196 (4)	296.728 351 (4)	33 691.0203 (6)	33 691.0204 (4)	
302.2	6p $^3P_2$	7d $^3D_3$	33 086.5095 (5)	302.149 987 (4)	33 086.5108 (5)	33 086.5114 (10)	
302.4	6p $^3P_2$	7d $^3D_2$			33 064.8824 (6)		
302.8	6p $^3P_2$	7d $^1D_2$			33 021.0535 (10)		
312.7	6p $^3P_1$	6d $^3D_2$	31 983.8669 (4)	312.567 019 (4)	31 983.8675 (5)	31 983.8676 (4)	
313.2	6p $^3P_1$	6d $^3D_1$	31 923.8026 (4)	313.155 133 (4)	31 923.8035 (5)	31 923.8035 (4)	
313.3	6p $^3P_1$	6d $^1D_2$	31 920.8368 (4)	313.184 230 (4)	31 920.8372 (5)	31 920.8374 (4)	
334.2	6p $^3P_1$	8s $^3S_1$	29 918.2418 (4)	334.148 163 (5)	29 918.2431 (4)	29 918.2434 (5)	
365.1	6p $^3P_2$	6d $^3D_3$	27 388.2792 (4)	365.015 686 (5)	27 388.2796 (4)	27 388.2799 (3)	cal
365.6	6p $^3P_2$	6d $^3D_2$	27 353.1900 (4)	365.483 947 (5)	27 353.1906 (4)	27 353.1908 (4)	
366.3	6p $^3P_2$	6d $^3D_1$	27 293.1261 (5)	366.288 288 (7)	27 293.1265 (6)	27 293.1270 (6)	
366.4	6p $^3P_2$	6d $^1D_2$	27 290.1596 (4)	366.328 105 (5)	27 290.1603 (4)	27 290.1603 (4)	
390.7	6p $^1P_1$	8d $^1D_2$			25 591.9547 (9)		
404.8	6p $^3P_0$	7s $^3S_1$	24 705.2982 (3)	404.657 161 (5)	24 705.2989 (4)	24 705.2989 (3)	cal, a
407.9	6p $^3P_1$	7s $^1S_0$	24 515.8758 (3)	407.783 818 (5)	24 515.8765 (4)	24 515.8766 (3)	
434.0	6p $^1P_1$	7d $^3D_2$	23 039.1116 (13)	433.922 520 (25)	23 039.1140 (6)	23 039.1141 (13)	
434.8	6p $^1P_1$	7d $^1D_2$	22 995.2820 (5)	434.749 603 (9)	22 995.2833 (3)	22 995.2836 (6)	
436.0	6p $^3P_1$	7s $^3S_1$	22 938.0812 (3)	435.833 759 (6)	22 938.0819 (3)	22 938.0820 (3)	cal, s, a
491.7	6p $^1P_1$	8s $^1S_0$	20 335.7736 (10)	491.607 015 (24)	20 335.7762 (5)	20 335.7763 (9)	
546.2	6p $^3P_2$	7s $^3S_1$	18 307.4042 (2)	546.075 330 (7)	18 307.4049 (3)	18 307.4050 (2)	cal, s
577.1	6p $^1P_1$	6d $^3D_2$	17 327.4230 (3)	576.959 855 (10)	17 327.4235 (4)	17 327.4237 (5)	s
579.2	6p $^1P_1$	6d $^1D_2$	17 264.3928 (3)	579.066 286 (11)	17 264.3927 (4)	17 264.3932 (7)	s

[a] Wavelength in air at standard temperature and pressure.
[b] Notes: cal—line used for calibration of the FTS wave number scale [20]; a—line of potential interest to astronomers [9]; s—line recommended as secondary wavelength standard [7].

satisfied. In table 2 our results for the wavelengths of these four standards, calculated from the regression analysis for 100 Pa argon pressure and temperature 8 °C, are compared to the CIPM recommended wavelengths. The agreement is excellent. Uncertainties are given at the 99% confidence level for direct comparison with the CIPM recommendations. Our data determine the wavelengths for three of these four lines with relative uncertainties better than the current CIPM recommended values.

3.2. Pressure shifts

3.2.1. Line shift and broadening. Since pressure shift and broadening of spectral lines take place due to atomic interactions, one can learn about underlying atom–atom interaction

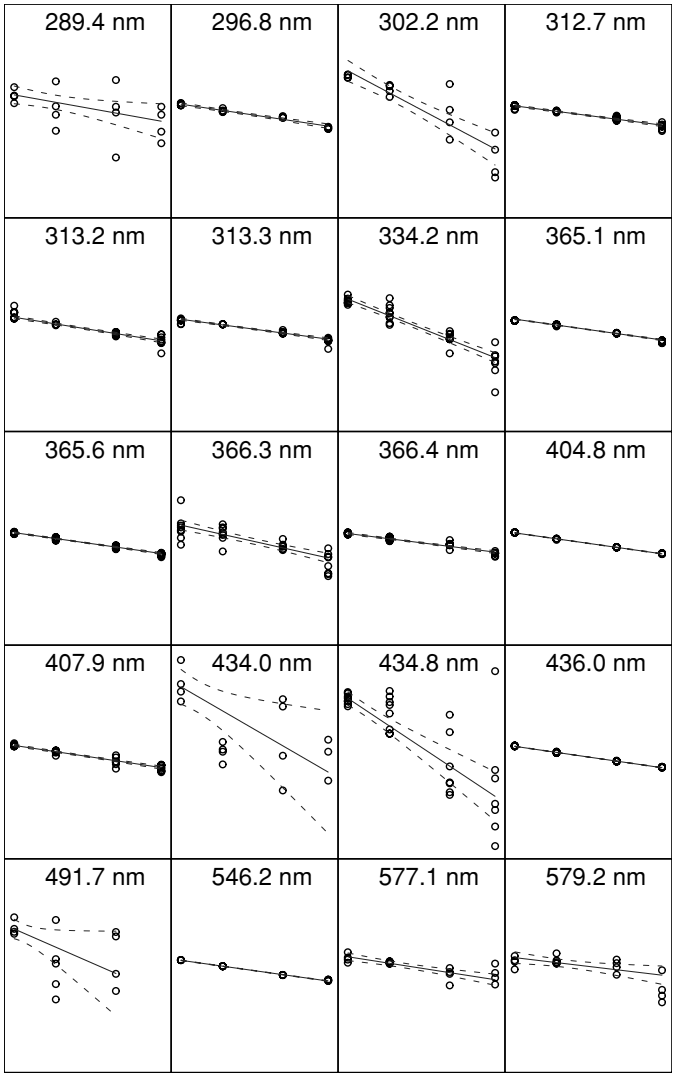

Figure 1. Dependence of wave numbers of 20 ^{198}Hg lines on argon pressure. For each subplot pressure is shown on the horizontal axis and the wave number on the vertical axis. Data points are shown at pressures of 33 Pa, 400 Pa, 933 Pa and 1333 Pa increasing to the right. For all lines the wave number data are mean-centred and the full height of the vertical axis represents 0.023 cm^{-1}. Broken curves correspond to the upper and the lower 95% confidence limits for the fit to the wave numbers.

potentials by analysing the pressure shift data. The redshift observed for all mercury lines (figure 1) indicates that the main contribution to the shift comes from the attractive long-range tail of the mercury–argon interatomic potential. In order to relate the line shifts determined in our experiment to the details of the atom–atom interactions, we will briefly review the theory of line shift and broadening.

Theories of line shift and broadening are usually divided into two limiting cases: the low-pressure impact collision limit, and the high-pressure statistical limit [15]. In the limit of low pressure the time between collisions is long compared to the duration of collisions, and

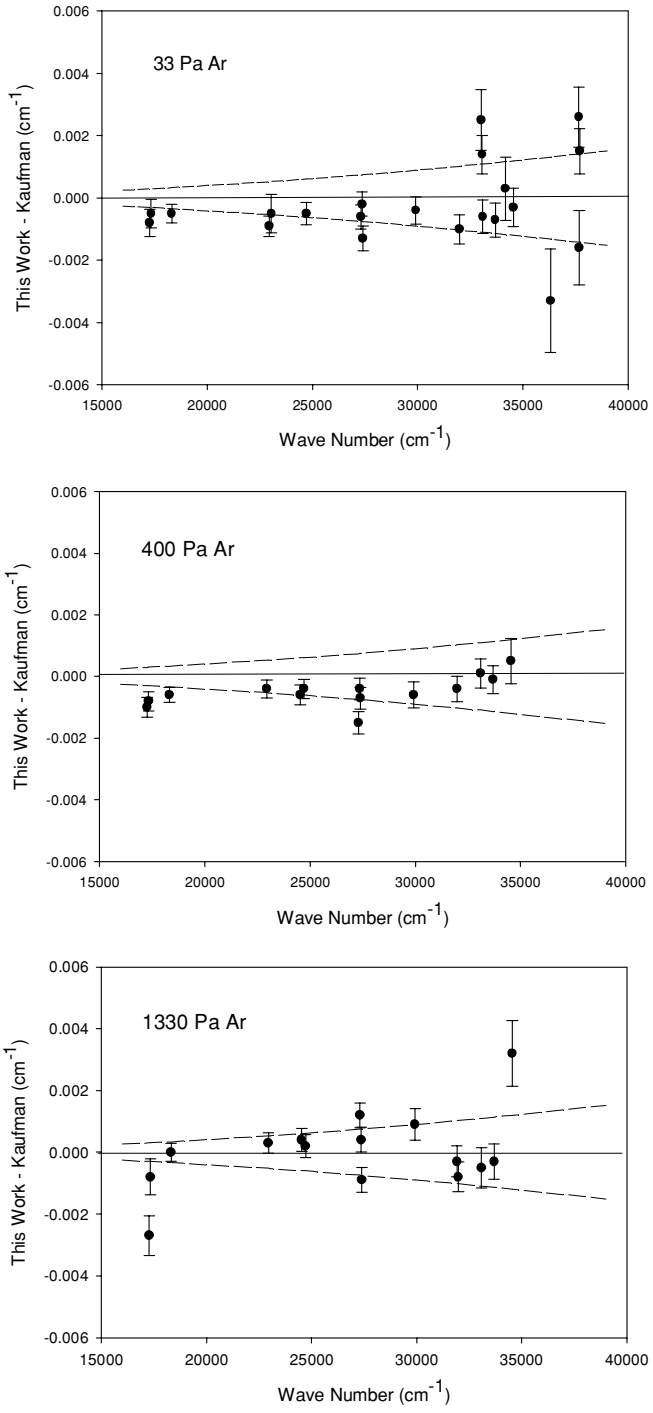

Figure 2. Comparison of wave numbers of 20 mercury emission lines measured in this experiment with measurements of Kaufman [4] in the lamps with 33 Pa, 400 Pa and 1333 Pa argon buffer gas. The broken line represents Kaufman's estimated overall uncertainty of ±0.00001 nm. The error bars represent the uncertainties of the wave numbers measured in this work at a 95% level of confidence.

Table 2. Comparison of the present results for ^{198}Hg with recommendations of the CIPM [7]. Uncertainties are given at the 99% confidence level for comparison with the CIPM recommendation.

CIPM recommended wavelength[a] (nm)	Relative uncertainty ($\times 10^{-8}$)	This work wavelength[b] (nm)	Relative uncertainty ($\times 10^{-8}$)
579.22 683 (3)	5.0	579.226 849 (35)	6.0
577.11 983 (3)	5.0	577.119 847 (25)	4.3
546.22 705 (3)	5.0	546.227 067 (10)	1.8
435.95 624 (2)	5.0	435.956 246 (8)	1.8

[a] For argon pressure between 66 Pa and 133 Pa.
[b] For argon pressure of 100 Pa, as derived from our measurements.

three-body (and higher order) collisions may be completely neglected. Thus, interactions affecting the line shift and the line shape can be understood through studies of binary atomic collisions. The collision is modelled as a scattering event, which depends on the relative motion between the active and the perturbing atom, as well as on the atom–perturber interaction potential. Our experiments were performed in the low-pressure regime, where the impact theory of line shift and broadening is valid. The fact that the line shifts shown in figure 1 all vary linearly with the perturber pressure is a clear indication that the impact approximation is valid over the range of pressures involved, since perturbation due to collisions is expected to be linearly proportional to the density of perturbing atoms in this approximation. However, the magnitude of the shift depends on the strength of the atomic interaction as well as on the number of collisions.

In the case of low-pressure foreign gas broadening, the Lindholm–Foley impact theory [12] predicts a Lorentzian line shape

$$L(\nu, \gamma, \beta) = \frac{\gamma}{\pi[(\nu - \nu_0 - \beta)^2 + \gamma^2]}, \tag{1}$$

where ν_0 is the centre frequency of the unshifted line, γ is the collision half-width at half-maximum (HWHM), and β is the collision-induced line shift. The quantities β and γ are given as [12]

$$\beta = v_{\mathrm{m}}\sigma_{\mathrm{I}}(v_{\mathrm{m}})N, \tag{2}$$

$$\gamma = v_{\mathrm{m}}\sigma_{\mathrm{R}}(v_{\mathrm{m}})N, \tag{3}$$

where σ_{I} and σ_{R} are the shift and broadening cross sections and N is the density of perturbing atoms. Here v_{m} denotes the mean relative velocity, $v_{\mathrm{m}} = (8k_{\mathrm{B}}T/\pi\mu)^{1/2}$, where k_{B} is the Boltzmann constant, T is the absolute temperature, and μ is the reduced mass of the colliding atoms. The ratios β/N and γ/N are known as the line shift and broadening constants (see the appendix).

In the framework of the same theory, the shift and broadening cross sections are given by [12]

$$\sigma_{\mathrm{I}}(v_{\mathrm{m}}) = 2\pi \int_0^\infty \sin\eta(\rho, v_{\mathrm{m}})\rho \,\mathrm{d}\rho, \tag{4}$$

and

$$\sigma_{\mathrm{R}}(v_{\mathrm{m}}) = 2\pi \int_0^\infty \{1 - \cos\eta(\rho, v_{\mathrm{m}})\}\rho \,\mathrm{d}\rho. \tag{5}$$

The quantity $\eta(\rho, v_m)$ is the total phase shift produced in a collision with an impact parameter ρ (the distance of the closest approach of the collision particles) and a mean relative velocity v_m,

$$\eta(\rho, v_m) = 2\pi \int_{-\infty}^{\infty} \{(2\pi)\Delta V[R(t)]/h\}\, dt. \tag{6}$$

Here

$$\Delta V(R) = V_u(R) - V_l(R) \tag{7}$$

is the difference interaction potential, $V_u(R)$ and $V_l(R)$ are the mercury–argon interaction potentials for the upper and the lower state of a transition in the mercury atom, and $R(t, \rho) = \left[\rho^2 + v_m^2 t^2\right]^{1/2}$ is the interatomic separation in the straight line approximation with t the time relative to the time of closest approach.

The total phase shift $\eta(\rho, v_m)$, and consequently all pressure shift (and broadening) data, depend on the nature of the interaction of the active and the perturber atoms. Collisions involving large impact parameters produce small phase changes of less than 1 rad, but are effective in shifting the mean wavelength of the spectral line. The effects of weak but frequent distant collisions are cumulative, so that small but numerous perturbations lead to a measurable shift of the line. On the other hand, strong collisions with small impact parameters considerably change the phase of radiation and are effective in producing the line broadening. Consequently, one can expect that the shift rates are much more sensitive to the real form of the difference potential than the broadening rates since they depend not only on the strength but also on the shape of the outer part of the interatomic potential.

3.2.2. The van der Waals interaction potential. The simplest suitable model for atomic interactions in the long-range region is the van der Waals potential $V(R) = -C_6\, R^{-6}$ ($C_6 > 0$) [12]. For this type of atomic interaction, the Lindholm–Foley theory yields the following expressions for the shift and broadening constants β/N and γ/N [11–14],

$$\beta/N = -2.96 v_m^{3/5} \left[\frac{2\pi\, \Delta C_6}{h}\right]^{2/5} \tag{8}$$

and

$$2\gamma/N = -2.76\beta/N. \tag{9}$$

The ΔC_6 constant appearing in equation (8) is known as an effective van der Waals constant, corresponding to the difference interaction potential of the type $\Delta V(R) = -\Delta C_6 R^{-6}$. The effective van der Waals constant ΔC_6 represents the difference of the van der Waals constants for the upper and the lower levels of the transition. The level van der Waals constant is often calculated according to the formula [24]

$$C_6 = \alpha_0 e^2 \langle r_k^2 \rangle, \tag{10}$$

where α_0 is the static polarizability of the perturber atom, e is the electron charge, and $\langle r_k^2 \rangle$ is the quantum mechanical expectation value of the mean square radius of the valence electron in state $|k\rangle$ of the radiating atom. In the case of a hydrogenic atom the mean square radius can be calculated exactly, using the Coulomb approximation, and is given by [24, 25]

$$\langle r_k^2 \rangle = \tfrac{1}{2} a_0^2 (n_k^*)^2 [5(n_k^*)^2 + 1 - 3l(l+1)], \tag{11}$$

where a_0 is the Bohr radius, n_k^* is the effective principal quantum number of the state $|k\rangle$, and l is the orbital angular momentum quantum number. This relation is widely used in calculations of van der Waals interaction constants, implicitly assuming that the Coulomb approximation

Table 3. Calculated mean square radii of the valence electron in excited states of ^{198}Hg and corresponding C_6 constants. The data are given in atomic units (au). The ionization potential of mercury is 84184.1 cm^{-1} [16].

		$\langle r_k^2 \rangle$ (au)[a]		C_6 (au)[b]	
Level	E (cm^{-1})	MCDF	CA	MCDF	CA
6p ^{3}P$_1$	39 412.300	17	9	187	99
6p ^{3}P$_0$	37 645.080	16	8	176	88
6p ^{3}P$_2$	44 042.977	21	12	231	132
6p ^{1}P$_1$	54 068.781	44	24	484	264
7s ^{3}S$_1$	62 350.456	79	66	869	726
7s ^{1}S$_0$	63 928.243	80	76	880	836
6d ^{1}D$_2$	71 333.182	137	110	1507	1210
6d ^{3}D$_1$	71 336.164	127	110	1397	1210
6d ^{3}D$_2$	71 396.220	128	111	1408	1221
6d ^{3}D$_3$	71 431.311	129	112	1419	1232
8s ^{3}S$_1$	73 961.298	324	293	3564	3223
8s ^{1}S$_0$	74 404.590	336	320	3696	3520
7d ^{1}D$_2$	77 064.097	536	463	5896	5093
7d ^{3}D$_2$	77 107.917	512	469	5632	5159
7d ^{3}D$_3$	77 129.535	516	473	5676	5203

[a] 1 au $= a_0^2$, where a_0 denotes the Bohr radius.
[b] 1 au $= a_0^5 e^2$, where e denotes the electron charge.

and hydrogenic wavefunctions can be used to describe valence states of complex atoms. The static polarizability of argon atoms is known rather accurately ($\alpha_0 = 11\ a_0^3\ \pm 10\%$, see [26] and references therein); therefore, the accuracy of the calculated van der Waals constant for a given level depends primarily on an accurate knowledge of the mean square radius of the valence electron. Since it can be calculated exactly only in the case of a hydrogenic atom, a calculation of this kind is of limited value for complex atoms, and the uncertainty is expected to be large for heavy elements and for atoms with more than one valence electron [12, 24, 25]. For example, in the case of Tl, the mean square radii for the 7s and 8p states calculated using Hartree–Fock or Dirac–Hartree–Fock wavefunctions are up to 50% larger than the same values calculated in the Coulomb approximation [27]. On the other hand, mean square radii for higher p and d states in He calculated using Hartree–Fock wavefunctions are about 30% smaller than the values calculated in Coulomb approximation [28]. Therefore, equation (11) may be too crude an approximation in the case of mercury. To check this possibility, we compared the $\langle r_k^2 \rangle$ calculated in the Coulomb approximation (CA) with values calculated from multiconfiguration Dirac–Fock (MCDF) wavefunctions [29]. The results are given in table 3. The MCDF and CA values of $\langle r_k^2 \rangle$ show a satisfactory agreement (within 20%) in the case of higher s and d levels. More significant differences exist in the case of the low-lying 6p ^{1}P$_J$ and 6p ^{3}P$_1$ levels, where the CA and MCDF calculations disagree by as much as a factor of 2. This result is in reasonable agreement with the case of Tl where the mean square radii for the high s and p states calculated using Dirac–Hartree–Fock wavefunctions are larger by a factor of 1.5 than the CA values [27]. We have accepted the values for $\langle r_k^2 \rangle$ calculated in the MCDF approximation as the more reliable results, and used the MCDF values for calculations of the C_6 constants and pressure shift constants.

C_6 constants calculated using equation (10) for both the CA and MCDF values for $\langle r_k^2 \rangle$ are given in table 3. Note that the effective van der Waals constants are heavily dominated by the upper state of the transition, since the $\langle r_k^2 \rangle$ of the valence electron is about an order of

magnitude larger in the upper level than in the lower level. Based on the comparison between CA and MCDF presented in table 3, and the estimates given in [12], one can expect that the calculation of $\langle r_k^2 \rangle$ has an overall accuracy of about ±20%. Since the static polarizability of argon atoms is known with a relative uncertainty of about ±10% one can expect that the calculated C_6 constants have an overall accuracy of about ±20% to ±30%.

We can use the information from table 3 to demonstrate *a posteriori* the validity of the binary and impact approximations in our experiment. First, all pressure shift measurements reported in this work were performed at a fixed discharge temperature of (8 ± 0.5) °C. At this temperature, the mercury vapour pressure is about 50 mPa (≈0.4 mTorr) [22]. Since the corresponding density of mercury atoms is about 1.4×10^{13} cm^{-3}, the binary approximation is clearly valid for lamps with argon densities between 8×10^{15} atoms cm^{-3} (33 Pa lamp) and 3.5×10^{17} atoms cm^{-3} (1333 Pa lamp). Second, according to [30], the impact approximation is valid if $N \ll 1/(\pi \rho_w^3)$, where ρ_w represents the Weisskopf radius [31] and N the perturber density. The Weisskopf radius is that impact parameter for which the collision phase shift $\eta(\rho)$ is 1 rad. It depends on the atomic interaction parameters as $\rho_w = (6\pi^2\, \Delta C_6/8\, h\, v_m)^{1/5}$ [31]. Since a typical value of the Weisskopf radius in the case of the mercury states of interest is about 1.5 nm, the inequality $N \ll 1/(\pi \rho_w^3)$ is always satisfied in our experiment. Therefore, the impact approximation for line shift and broadening is valid under our experimental conditions.

3.2.3. The Lennard–Jones interaction potential. The Lennard–Jones potential is often chosen as an alternative to the van der Waals potential as a model atomic interaction potential [11, 12]. This potential is given by $V(R) = C_{12}R^{-12} - C_6R^{-6}$ ($C_6 > 0, C_{12} > 0$). Generally, it is a more realistic model for atomic interactions, taking into account not only the long-range attraction but also a strong repulsion at smaller distances.

The C_6 constants for the Lennard–Jones potential are given by equation (10), and the C_{12} constants are calculated according to the Kielkopf empirical formula [15]

$$C_{12} = A(n_k^*)^B, \tag{12}$$

where $A = 8.6 \times 10^{-105}$ erg cm^{12}, and $B = 10.2$. Kielkopf showed that this simple formula gives satisfactory results in the case of heavy noble gases (Ar, Kr, Xe). Unfortunately, the estimated relative error of this approximation is rather high, reaching about 25% [15]. Nevertheless, to assess the influence of a repulsive term on the long-range tail of the van der Waals potential (outer part of the interatomic potential responsible for the line shifts), we performed additional calculations of the line shifts using the Lennard–Jones interaction potential. For this type of atomic interaction the Lindholm–Foley theory of impact line broadening yields the following expressions for the line shift and broadening constants [11]:

$$\beta/N = 2\pi \left(\frac{3\pi}{8}\right)^{2/5} S(\alpha) v_m^{3/5} \left[\frac{2\pi \Delta C_6}{h}\right]^{2/5}, \tag{13}$$

$$2\gamma/N = 4(\beta/N)[B(\alpha)/S(\alpha)], \tag{14}$$

$$\alpha = \frac{63\pi}{256}\left(\frac{8}{3\pi}\right)^{11/5}\left(\frac{h v_m}{2\pi}\right)^{6/5} \Delta C_{12} |\Delta C_6|^{-11/5}. \tag{15}$$

The dimensionless functions $S(\alpha)$ and $B(\alpha)$ have been tabulated by Hindmarsh *et al* [11]. The ΔC_{12} constant appearing in equation (15) is an effective constant, corresponding to the Lennard–Jones difference interaction potential of type $\Delta V(R) = \Delta C_{12}R^{-12} - \Delta C_6 R^{-6}$, where ΔC_{12} represents the difference of C_{12} constants for the upper and the lower levels of the transition. Note that effective ΔC_{12} constants are also heavily dominated by the upper state of

Table 4. Argon pressure shift rates (PSR), shift constants ($\Delta\nu_0/N$) and shift cross sections (σ_1) measured in this experiment compared to the measurements reported by Salit *et al* [20] and Kaufman [4]. Uncertainties are given at a 95% level of confidence.

			Pressure shift rates (PSR) ($\times 10^{-6}$ cm^{-1}/Pa)			Pressure shift constants ($\Delta\nu_0/N$) ($\times 10^{-21}$ cm^{-1}/cm^{-3})		Pressure shift cross sections (σ_1) ($\times 10^{-14}$ cm^2)
	Level							
Line	Lower	Upper	[4]	[20]	Experiment (this work)	Experiment (this work)	Calculation[a] (this work)	Experiment (this work)
289.4	6p ^{3}P$_1$	8s ^{3}S$_1$	−4		−2.23 ± 1.68	−8.67 ± 6.52	−14.68	3.86 ± 2.90
296.8	6p ^{3}P$_0$	6d ^{3}D$_1$	−3		−2.03 ± 0.28	−7.86 ± 1.09	−9.77	3.50 ± 0.49
302.2	6p ^{3}P$_2$	7d ^{3}D$_3$	−6		−5.48 ± 1.46	−21.25 ± 5.66	−17.77	9.46 ± 2.52
312.7	6p ^{3}P$_1$	6d ^{3}D$_2$	−2		−1.81 ± 0.19	−7.02 ± 0.72	−9.77	3.12 ± 0.32
313.2	6p ^{3}P$_1$	6d ^{3}D$_1$	−4		−2.16 ± 0.25	−8.39 ± 0.97	−9.73	3.74 ± 0.43
313.3	6p ^{3}P$_1$	6d ^{1}D$_2$	−2		−1.86 ± 0.17	−7.20 ± 0.67	−10.08	3.21 ± 0.30
334.2	6p ^{3}P$_2$	8s ^{3}S$_1$	−4		−4.58 ± 0.54	−17.78 ± 2.09	−14.60	7.92 ± 0.93
365.1	6p ^{3}P$_2$	6d ^{3}D$_3$	−3	−1.73 ± 0.33	−1.94 ± 0.09	−7.54 ± 0.34	−9.66	3.36 ± 0.15
365.6	6p ^{3}P$_2$	6d ^{3}D$_2$	−2		−1.95 ± 0.13	−7.55 ± 0.49	−9.63	3.36 ± 0.22
366.3	6p ^{3}P$_2$	6d ^{3}D$_1$	−3		−2.86 ± 0.66	−11.09 ± 2.56	−9.59	4.94 ± 1.14
366.4	6p ^{3}P$_2$	6d ^{1}D$_2$			−1.75 ± 0.19	−6.78 ± 0.72	−9.94	3.02 ± 0.32
404.8	6p ^{3}P$_0$	7s ^{3}S$_1$	−2	−1.94 ± 0.31	−1.96 ± 0.05	−7.59 ± 0.19	−7.74	3.38 ± 0.08
407.9	6p ^{3}P$_1$	7s ^{1}S$_0$	−2		−2.05 ± 0.20	−7.95 ± 0.78	−7.79	3.54 ± 0.35
434.0	6p ^{1}P$_1$	7d ^{3}D$_2$	−6		−5.07 ± 3.69	−19.67 ± 14.3	−17.37	8.76 ± 6.37
434.8	6p ^{1}P$_1$	7d ^{1}D$_2$	−4		−6.26 ± 1.67	−24.30 ± 6.49	−17.72	10.82 ± 2.89
436.0	6p ^{3}P$_1$	7s ^{3}S$_1$	−3	−1.97 ± 0.30	−1.99 ± 0.05	−7.74 ± 0.18	−7.69	3.45 ± 0.08
491.7	6p ^{1}P$_1$	8s ^{1}S$_0$			−4.63 ± 4.24	−17.96 ± 16.47	−14.38	8.00 ± 7.33
546.2	6p ^{3}P$_2$	7s ^{3}S$_1$	−2	−1.83 ± 0.24	−1.94 ± 0.04	−7.52 ± 0.16	−7.48	3.35 ± 0.07
577.1	6p ^{1}P$_1$	6d ^{3}D$_2$	−1		−2.07 ± 0.68	−8.04 ± 2.66	−8.74	3.58 ± 1.18
579.2	6p ^{1}P$_1$	6d ^{1}D$_2$			−1.60 ± 1.10	−6.21 ± 4.26	−9.10	2.76 ± 1.90

[a] Assuming van der Waals interaction and $\langle r^2\rangle$ calculated in MCDF approximation.

a transition, since the C_{12} constant for the upper level is about one order of magnitude larger than the C_{12} constant for the lower level. In the limit of a pure van der Waals interaction (i.e., if $C_{12} \to 0$ and $\Delta C_{12} \to 0$) equations (13) and (14) smoothly reduce to equations (8) and (9).

3.2.4. Discussion of the pressure shift data. In table 4, we summarize our observed argon pressure shifts. In the same table, we compare the argon pressure shift constants (determined from the pressure shift rates) with the pressure shift constants calculated in the MCDF approximation. We also give a list of argon pressure shift cross sections determined from the pressure shift rates

In the first part of table 4, the argon pressure shift rates measured in this experiment are compared to those measured in our earlier experiment [20] and by Kaufman [4]. The reported uncertainties are expanded to provide a 95% confidence level. Our results are in satisfactory agreement with those of Kaufman. Although no uncertainties are given in [4], we assume that the average uncertainty of these data is about 20% since the pressure shift rates are given as single digit numbers. Since Kaufman's results have a slight bias to higher wave numbers at lower argon pressures (figure 2), the shift rates given by [4] are on average larger than our measurements. The new values for the shift rates of the four strongest mercury lines are in excellent agreement with our earlier results [20], but have uncertainties that are smaller by a factor of approximately 6. In our previous experiment, the light from the Hg lamp and calibration laser was collected by an integrating sphere mounted in front of the entrance aperture of the FTS in order to obtain a uniform illumination of the aperture from the two very different light sources. The large loss of light in the integrating sphere reduced the SNR in the spectra limiting the uncertainty of the measurements.

In the last part of table 4, we list the measured and the calculated pressure shift constants, as well as the pressure shift cross sections. The uncertainties of the measured pressure shift

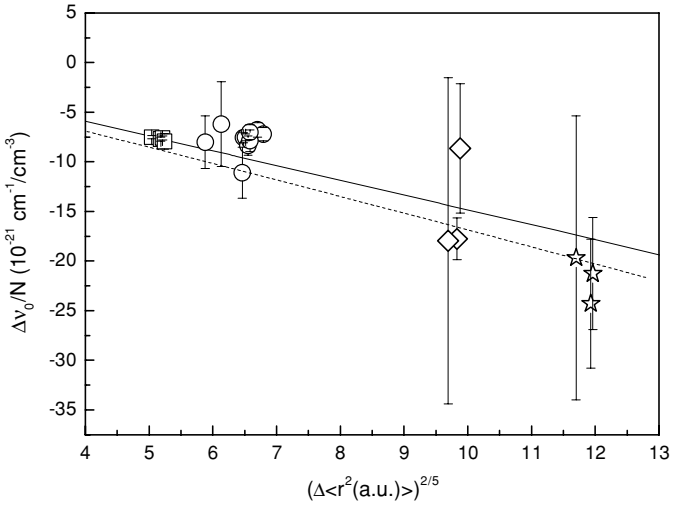

Figure 3. Comparison of the calculated and measured argon pressure shift constants for 20 lines of ^{198}Hg. Solid line: calculated shift constants based on a van der Waals interaction potential; broken curve: calculated shift constants based on a Lennard–Jones interaction potential; squares: transitions with 7s upper states; circles: transitions with 6d upper states; diamonds: transitions with 8s upper states; stars: transitions with 7d upper states. The error bars of the measured pressure shift constants are given at a 95% level of confidence.

constants and shift cross sections are derived from the uncertainties of the measured pressure shift rates. The measured and the calculated pressure shift constants are graphically presented in figure 3, in order to facilitate the comparison between theory and experiment. The abscissa represents the quantity $(\Delta\langle r^2\rangle)^{2/5}$, and the ordinate corresponds to the pressure shift constant $\Delta\nu_0/N$. Plotting the data in this way leads to a linear dependence in the case of pure van der Waals interaction potentials (see equation (8)).

The bold straight line in figure 3 represents the shift constants calculated using the van der Waals interaction potential. The dashed slightly curved line is a trend curve, representing the set of shift constants calculated using the Lennard–Jones interaction potential (actual calculated points are scattered around this curve). Open squares denote the experimental shift constants for transitions with 7s upper states, circles for transitions with 6d upper states, diamonds for transitions with 8s upper states, and stars for transitions with 7d upper states. It is clear that the shifts of the lines that have upper states in the same configuration, but lower states in different configurations, are similar (or even equal) within experimental error. Their similarity indicates that variation of the lower state interaction potential exerts only a small effect compared with that of the excited state.

The transitions with 7s upper states agree very well with the van der Waals result. However, seven of the ten lines with 6d upper states disagree significantly outside the 95% experimental confidence interval. In addition, the best determined 7s and 6d points fall in two tight clusters that suggest a corresponding trend line that is flat or even has a slightly positive slope as compared to the negative (nearly equal) slopes produced by the van der Waals and Lennard–Jones potentials. Attributing a 30% uncertainty to the theory, however, the absolute agreement between theory and experiment is satisfactory. For the transitions with 8s and 7d upper levels, the experimental uncertainties are so large that it seems difficult to draw any firm conclusion about agreement with the theory from the marginally better agreement with the Lennard–Jones results.

Since the Lennard–Jones results do not differ appreciably from the van der Waals calculations, it appears that a simple van der Waals interaction picture provides an adequate description of the long-range part of the excited mercury–argon interatomic potentials. However, it is possible that a better representation of the interaction potentials of excited mercury atoms with argon could be obtained using a 3-parameter potential of type C_6–C_8–C_{12}, or potentials which are a superposition of a polarization potential and a Fermi potential [32]. It is obvious that more sophisticated calculations, and perhaps additional experiments, are needed to determine atomic interaction potentials for highly excited mercury atoms perturbed by argon.

4. Conclusions

We measured wave numbers and collision-induced shifts of ^{198}Hg emission lines using Fourier transform spectroscopy. The measurements were made using electrodeless lamps containing the single isotope ^{198}Hg and argon buffer gas at four different pressures. Accurate calibration of the FTS wave number scale, obtained using the four most prominent ^{198}Hg emission lines, enabled determination of wave numbers of UV and visible mercury emission lines with high accuracy. The wave numbers of mercury lines emitted from the 400 Pa lamp are useful wavelength standards for calibration in ICP spectrochemical analysis, in experiments where medium-resolution monochromators are used, and for Fourier transform spectroscopy and other interferometric experiments.

The measured pressure shifts of the ^{198}Hg emission lines are in reasonable agreement with theoretical predictions. The measurements suggest that the interaction of excited mercury atoms with argon can be acceptably described by a simple van der Waals potential. Nevertheless, calculations of the atomic interaction potentials of Hg–Ar based on a more sophisticated theoretical approach are needed to interpret the broadening and shift of mercury lines in the general case.

Acknowledgments

The authors gratefully acknowledge Yong-Ki Kim of NIST and Jean-Paul Desclaux for their help in calculating mean square radii in the MCDF approximation for this work. Damir Veza gratefully acknowledges the hospitality of the NIST Atomic Spectroscopy Group.

Appendix

The pressure shift and broadening constants are quoted in different forms in the literature. Most frequently they are given in the units of $\mathrm{cm}^{-1}/(\mathrm{atoms\ cm}^{-3})$ [13] or $\mathrm{s}^{-1}/(\mathrm{atoms\ cm}^{-3})$ [15]. If the line width and the line shift are expressed in cm^{-1}, the designation is usually $\Delta\nu_{1/2}$ for the full line width at half intensity (FWHM), and $\Delta\nu_0$ for the line shift [13]. If expressed in s^{-1} the common designation is γ (or w) for the line half-width at half intensity (HWHM) and β (or d) for the line shift. The two different notations are related as [13]

$$\beta/N = 2\pi c\frac{\Delta\nu_0}{N} \tag{A1}$$

and

$$2\gamma/N = 2\pi c\frac{\Delta\nu_{1/2}}{N}. \tag{A2}$$

However, the pressure shift and broadening constants depend not only on the nature of the atomic interactions, but also on the gas temperature and atomic masses. The presentation of the pressure broadening and shift data only in the form of pressure shift and broadening constants obscures their temperature and mass dependence. Consequently, it is useful to present the same data as shift and broadening cross sections, σ_{I} and σ_{R}, derived from the pressure shift and broadening constants via the expressions [13]

$$\sigma_I = \frac{\beta/N}{v_{\mathrm{m}}} \tag{A3}$$

and

$$\sigma_R = \frac{\gamma/N}{v_{\mathrm{m}}}. \tag{A4}$$

The pressure shift and broadening cross sections are usually given in cm^{-2}.

References

[1] Meggers W F 1948 *J. Opt. Soc. Am.* **38** 7
[2] Engelhard E 1962 *Comité Consultatif pour la Définition du Mètre* (Paris: Gauthier-Villars)
[3] Meggers W F and Kessler K G 1950 *J. Opt. Soc. Am.* **40** 737
[4] Kaufman V 1962 *J. Opt. Soc. Am.* **52** 866
[5] Salit M L, Travis J C and Winchester M R 1996 *Appl. Opt.* **35** 2960
[6] Reader J, Sansonetti C J and Bridges J M 1996 *Appl. Opt.* **35** 78
[7] Quinn T J 2003 *Metrologia* **40** 103
[8] Sansonetti C J, Salit M L and Reader J 1996 *Appl. Opt.* **35** 74
[9] Wahlgren G M, Dolk L, Kalus G, Johansson S, Litzén U and Leckrone D S 2000 *Astrophys. J.* **539** 908
[10] Chen S Y and Takeo M 1957 *Rev. Mod. Phys.* **29** 20
[11] Hindmarsh W R and Farr J M 1972 *Prog. Quantum Electron.* **2** 141
[12] Schuller F and Behmenburg W 1974 *Phys. Rep.* **12** 273
[13] Lewis E L 1980 *Phys. Rep.* **58** 1
[14] Peach G 1981 *Adv. Phys.* **30** 367
[15] Allard N and Kielkopf J 1982 *Rev. Mod. Phys.* **54** 1103
[16] http://www.physics.nist.gov/PhysRefData/contents-atomic.html
[17] Thorne A P, Harris C J, Wynne-Jones I, Learner R C M and Cox G 1987 *J. Phys. E: Sci. Instrum.* **20** 54
[18] Thorne A P 1991 *Anal. Chem.* **63** 57 A
[19] Travis J C, Winchester M R and Salit M L 1993 *Spectrochim. Acta* **48 B** 691
[20] Salit M L, Sansonetti C J, Veza D and Travis J C 2004 *J. Opt. Soc. Am.* B **21** 1543
[21] Fehsenfeld F C, Evenson K M and Broida H P 1963 *Rev. Sci. Instrum.* **36** 294
[22] Honig R E and Kramer D A 1969 *RCA Rev.* **30** 285
[23] Sansonetti C J 1997 *J. Opt. Soc. Am.* B **14** 1913
[24] Unsőld A 1955 *Physik der Sternatmosphären* (Berlin: Springer)
[25] Bethe H A and Salpeter E E 1977 *Quantum Mechanics of One- and Two-Electron Atoms* (New York: Plenum)
[26] DeWitt M J, Prall B S and Lewis R J 2000 *J. Chem. Phys.* **113** 1553
[27] Dygdala R S, Lisicki E and Szudy J 1987 *J. Phys.* B **20** 3001
[28] Bielski A and Wolnikowski J 1978 *Acta Phys. Pol.* A **54** 601
[29] Kim Y-K 2005 private communication
[30] Baranger M 1962 *Atomic and Molecular Processes* ed D R Bates (New York: Academic) p 493
[31] Thorne A, Litzén U and Johansson S 1999 *Spectrophysics* (Berlin: Springer)
[32] Kaulakys B 1984 *J. Phys. B: At. Mol. Phys.* **17** 4485